Proceedings of the ASME 2014 33rd International Conference on Ocean, Offshore and Arctic Engineering
OMAE2014
June 8-13, 2014, San Francisco, California, USA

OMAE2014-24472

THE IDENTIFICATION OF POWER-IN REGION IN VORTEX-INDUCED VIBRATION OF FLEXIBLE CYLINDERS

Zhibiao Rao[1]
Department of Mechanical Engineering
Massachusetts Institute of Technology
Cambridge, MA, USA

Themistocles L. Resvanis
Department of Mechanical Engineering
Massachusetts Institute of Technology
Cambridge, MA, USA

Prof. J. Kim Vandiver
Department of Mechanical Engineering
Massachusetts Institute of Technology
Cambridge, MA, USA

[1] Corresponding Author, Zhibiao Rao, Email: zbrao@mit.edu

ABSTRACT

This paper proposes a novel method to identify the power-in regions of long flexible cylinders subjected to vortex-induced vibration (VIV). It also attempts to address a practical problem: "Will a secondary power-in region appear after the primary power-in region is covered with suppression devices?" The source of data is a recent model test on a 38 meter long flexible cylinder, densely instrumented with fiber optic strain gauges and accelerometers.

For pipes with partial coverage of suppression devices in uniform flow, the bare region would be expected to be a power-in region and the section with suppression devices is expected to be a power-out region. Experimental data from these types of tests are used to benchmark the proposed power-in zone identification method. The method is then used to identify the power-in zones on a bare cylinder in a sheared flow.

This paper also explores the occurrence of secondary power-in regions that may exist, when suppression devices are placed in the primary power-in zone. Secondary power-in regions were observed. Lessons learned from the power-in region identification in sheared flows will be a useful tool for designer/engineers choosing where to place suppression devices.

INTRODUCTION

Vortex-Induced Vibration (VIV) may result in significant fatigue damage on exploration and production risers used in the offshore industry. The regions where the shedding of vortices is correlated with the structural responses are designated power-in regions. Regions on the pipe that are not a source of power are designated power-out regions. A series of VIV model tests were conducted by SHELL Exploration and Production in March 2011(MARINTEK, 2011) to study the effect of various power-in lengths on VIV. Partial experimental results were published in Rao et al. (2012, 2013), Resvanis et al. (2012, 2014) and Jhingran et al. (2012). Three different 38m long riser models with various outer diameters and varying amounts of suppression devices were tested at different speeds in uniform and linearly sheared flow. The primary objective of this paper is to present a method for the identification of power-in regions on long flexible cylinders with a variety of flow profiles.

Swithenbank and Vandiver (2007) pioneered methods for locating the power-in region of long flexible cylinders, using data from two tests conducted in the Gulf Stream. Two methods, the coherence mesh and the reduced velocity, were presented to locate the source of VIV. The coherence mesh method is based on the assumption that the large amplitude travelling waves are expected to be coherent over a long range. This method fails to locate the power-in region when VIV response is dominated by standing waves. The reduced velocity method is based on the assumption that reduced velocity range from 5 to 7 is associated with large VIV response and is assumed to be a power-in region. However, the reduced velocity method fails when the pipe is partially covered with suppression devices under uniform flow. This is because the suppression devices are able to cause the region to be power-out, even when the reduced velocity is in the 5 to 7 range.

This paper proposes a methodology based on energy conservation to identify the power-in regions of long flexible cylinders from experimental data. The region associated with positive time average power is considered the power-in region. This method is more robust than those proposed by Swithenbank & Vandiver. It doesn't require the dominance of traveling wave and works for the pipe partially covered with suppression devices under uniform and sheared flows.

Once one understands where power-in regions occur, one may develop strategies for deploying suppression devices on flexible cylinders. The application of suppression devices naturally leads to the question "Will secondary power-in regions exist, after covering the original power-in region with suppression devices?"

The above question is answered by studying another VIV model test. ExxonMobil (EM) Upstream Research Company (URC) conducted a series of VIV model tests in 2003 to study the effect of various amounts of strakes coverage on a pipe in sheared flow. Here it is referred to as the EM URC test. Pipes were tested with strakes covering higher speed region of sheared flow. These tests revealed that when the higher speed regions are covered with suppression devices, secondary power-in regions develop. Four pipes with varying amounts of helical strakes in identical sheared flows were studied:

- 100% bare pipe with sheared flow
- The same pipe with 25% continuous helical strakes applied to the higher flow speed end
- The same pipe with 50% continuous helical strakes applied to the higher flow speed end
- The same pipe with 75% continuous helical strakes applied to the higher flow speed end

The main objectives of this paper are to:

1) Present a method for identifying power-in regions for cylinders in both uniform and sheared flows.
2) Study the change of power-in locations with the coverage of helical strakes.
3) Explore the occurrence of secondary power-in regions when the primary power-in zone is suppressed

EXPERIMENT DESCRIPTION

The research on the power-in region identification topic is based on two VIV experimental datasets. The first are SHELL tests and the other are EM URC tests.

SHELL TESTS The VIV experiments were conducted by SHELL Exploration and Production in March 2011 in the MARINTEK Offshore Basin in Trondheim, Norway. The main objectives of the SHELL test campaign were to explore effects on VIV of varying amounts of suppression devices and marine growth. Three 38-meter-long riser models were tested with different diameters. Pipe 1 had a diameter of 12mm and was made of a rod of fiberglass and polyester. Pipe 2 was a 30mm diameter fiberglass reinforced polyester tube. Pipe 3 used Pipe 2 as the inner core. Clamshell modules, 80mm in diameter were clamped onto the outside of 30mm inner pipe.

All pipes in the SHELL test were densely instrumented with 52 fiber optic strain sensors and accelerometers. Pipe 1 was instrumented with only fiber optic strain gauges at 52 equidistant locations. The fibers were glued outside the fiberglass rod, in four quadrants of the cross section to capture bending in two planes. The fibers were protected by an outer silicon rubber layer. Pipe 2/Pipe 3 was instrumented similarly as Pipe 1 with FBG strain gauges at 30 equidistant locations. Additional 22 bi-axial accelerometers were mounted on Pipe 2/Pipe 3 in order to measure IL and CF accelerations. Additionally, two tri-axial force transducers were installed at both ends. All transducers were sampled at a rate of 1200Hz.

EM URC TESTS In 2003, EM URC conducted a laboratory test at MARINTEK using a 10m model of a top tensioned riser. A fixture rotated the tensioned riser along a circular path in still water. The model could be oriented vertically or inclined to simulate a linearly varying current distribution. The model was a 20mm diameter brass pipe with a length of 9.63m. The maximum Reynolds number was 50,000. The model was heavily instrumented as shown in Fig. 5 with strain gauges and accelerometers to resolve up to mode 8 in the cross-flow direction and mode 16 in the in-line direction. Additional details about the test are provided in Tognarelli et al (2004) and Campbell and Slocum (2013).

Material properties of pipes are given in details in the Table 1.

Table 1: Tested Pipe Properties

Parameters	SHELL TEST		EM URC TEST
	Pipe 1	Pipe 3	Pipe 4
Length (m)	38.00	38.00	9.63
Hydro diameter (m)	0.012	0.080	0.020
Strength diameter (m)	0.010	0.027	0.019
Inner diameter (m)	0	0.021	0
Bending stiffness (Nm^2)	16.1	572.3	135.4
Young modulus (N/m^2)	3.27×10^{10}	3.46×10^{10}	1.025×10^{11}
Mass in air (kg/m)	0.197	5.708	0.699
Mass ratio	1.74	1.14	2.23

• Bare Pipe 1

Bare Pipe 1 was tested in linearly sheared flows. The maximum flow speed was up to 3.1m/s corresponding to a Reynolds number of ~37200.

• Pipe 1 with Ribbon Fairings

The ribbon fairings were installed symmetrically towards both ends of Pipe 1, leaving a gap in the middle. The gap was 5%,

10%, 15% and 25% of the total length of Pipe 1. A picture of Pipe 1 with fairings is shown in Fig.1. All tests were performed in uniform flow. The maximum flow speed was up to 1.5m/s corresponding to a Reynolds number of ~18 000.

Figure 1. Pipe 1 covered with ribbon fairings

• Bare Pipe 3 with Triple Start Helical Strakes

The triple start helical strakes were cast from polyurethane, and were delivered in sections 430mm in length. Each complete section was made up of two half-shells attached to the 80mm pipe with plastic straps. The thickness of the half-shell was 3mm, making the outer diameter for the shells equal to 86mm. The helical strakes protruded an additional 25% of the 86mm diameter. The pitch was equal to 15 diameters. The strake sections were mounted to the pipe with plastic straps. The strakes were close to neutrally buoyant.

• Bare Pipe 3 Fully Covered with Strakes and 30% Soft Marine Growth

Marine growth was added onto the fully straked Pipe 3. The marine growth was 30% of the fin height and is referred to as 30% marine growth.

This pipe was investigated in sheared flows. The flow speed varied from 0.25 - 3.0m/s. A picture of fully straked Pipe 3 with 30% marine soft growth is shown in Fig. 2.

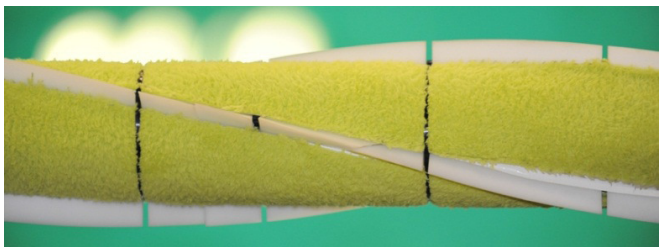

Figure 2. Fully straked Pipe 3 with 30% marine growth

• Bare Pipe 3 Fully Covered with Strakes and 60% Soft Marine Growth

In this set of experiments, the marine growth was changed to 60% of the strake height. This fully straked pipe was investigated in sheared flows. The flow speed varied from 0.25 - 2.5m/s.

• Bare Pipe 3 Fully Covered with Strakes of Which 60% Was Covered with 60% High Soft Marine Growth

Bare Pipe 3 was fully covered with helical strakes. 60% of the strakes were covered by 60% fin-height marine growth, leaving 40% covered with clean strakes. This pipe was investigated in sheared flows. The flow speed ranged from 0.25-2.5m/s. And the marine growth was at the higher flow speed end.

• Bare Pipe 4 (EM URC TEST)

Bare Pipe 4 tested in linear sheared flows in EM URC Test. The maximum velocity was 2.38m/s corresponding to a Reynolds number of ~47000.

• Pipe 4 with Triple Start Helical Strakes

Continuous triple start helical strakes with a height equal to 25% of the cylinder diameter and a pitch of 16 diameters were fitted to bare Pipe 4. Three different strake coverages of 25%, 50% and 75%, were tested in sheared flow. The strakes were installed at the higher flow speed end. The maximum rotating velocity was varied from 0.2-2.38m/s with the corresponding Reynolds number range was 4000-47000.

PHENOMENA OBSERVED

Observed VIV Frequency Content

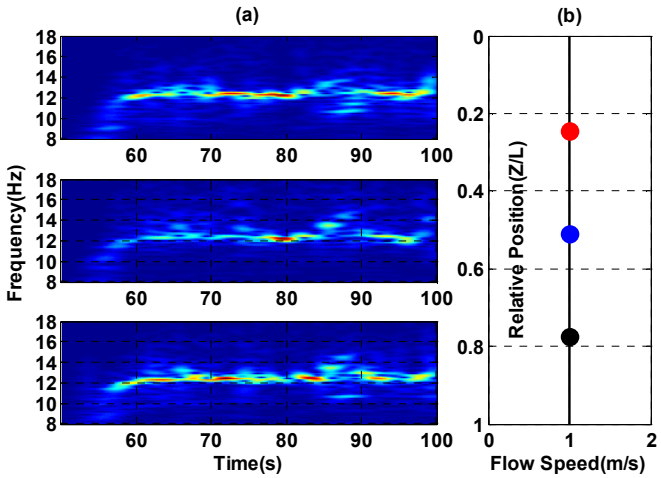

Figure 3(a) Time-Frequency plots for Test 2331 show that steady state conditions are achieved after 60 seconds. 3(b) The current profile annotated with the locations of the sensors used to gather the data shown in 3(a).

Figure 3 (a) presents data from Pipe 1 with a gap in the ribbon fairing of 15% in the center at 1m/s uniform flow speed (Test 2331). The left three plots are time-frequency plots, also called scalograms, at three different axial locations, with *Z/L* coordinates of 0.25, 0.51 and 0.77 which corresponds to sensor 13, 27 and 41 respectively. These locations are shown in Fig.3 (b) with three colored dots on the current profile. The top and bottom sensors were in the faired regions and the middle sensor location was in the bare region. The scalograms are plotted with a Complex Morlet function in MATLAB.

These scalograms indicate that the fundamental frequency of VIV was not constant for the duration of the test. They suggest that the frequency varied significantly before 60 seconds and after 85 seconds. From 60 to 85 seconds, the frequency changes very slowly. This period is assumed to be in a steady state condition. The dominant frequency in the steady state region is approximately 12.6Hz.

Observed Traveling Wave Response

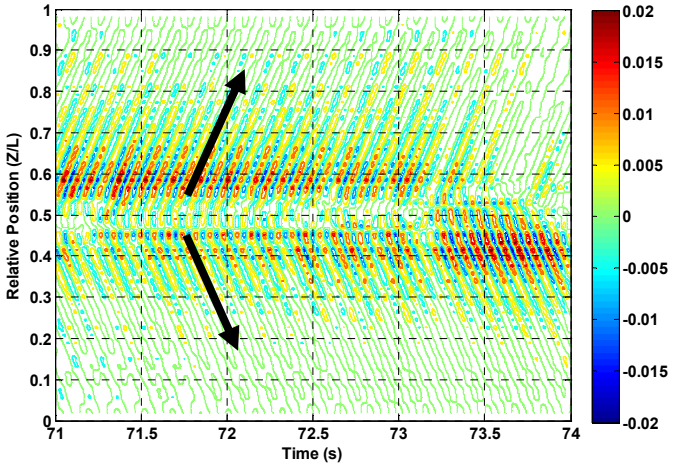

Figure 4. Time series contour plot of band-pass-filtered curvature measured at all 52 locations along the pipe for Test 2331.

Figure 4 shows a contour plot of measured curvature at all 52 locations for a short time window. The curvature time histories were band-passed filtered from 6.3Hz to 18.9Hz. A short time section between 70.9 to 73.1 seconds was chosen from the steady state time section identified above. The plot shows the amplitude of measured curvature, expressed in color, as a function of time (horizontal axis). The vertical axis is relative position along the entire length of the cylinder. The response is dominated by traveling waves, as indicated by the non-vertical slope of contours of constant color. It is clearly seen that there are two traveling waves emanating from the exposed region which is in the centre of the pipe. One wave is traveling upward and the other is traveling downward. That is to be expected, when the exposed, bare region is in the centre of the pipe as in this model test. The exposed region is a power-in region which absorbs energy from the flow, and the faired regions are the power-out regions which dissipate VIV energy. Waves emanating from the power-in region travel into the faired region, where they attenuate due to damping.

METHODOLOGY TO IDENTIFY POWER-IN REGIONS

The Equation of Motion of a Flexible Riser

The equation of motion describing the vortex-induced vibration of a flexible riser may be written as:

$$\boldsymbol{m}\frac{\boldsymbol{d^2v(z,t)}}{\boldsymbol{dt^2}}+\boldsymbol{c(z)}\frac{\boldsymbol{dv(z,t)}}{\boldsymbol{dt}}+\boldsymbol{EI}\frac{\boldsymbol{d^4v(z,t)}}{\boldsymbol{dz^4}}-\boldsymbol{T}\frac{\boldsymbol{d^2v(z,t)}}{\boldsymbol{dz^2}}=\boldsymbol{F(z,t)} \quad (1)$$

Where *m, EI,* and *T* are the constant mass per unit length, bending stiffness and tension, respectively; *v(z, t)* is the displacement in the cross-flow direction; *c(z)* is the damping per unit length; *F(z, t)* is the excitation force in Newton per unit length.

In equation (1), the hydrodynamic contribution to the damping term, *c(z)*, is assumed to come only from the power-out region. The excitation force per unit length *F(z, t)* is assumed to act only in the power-in region.

Equation (1) is difficult to evaluate directly because one does not usually have measurements of the damping or external excitation forces. Therefore in this paper the problem is restated in forms of energy conservation, which provides an alternative means of estimating the effects of lift force and damping.

Energy Density and Flux

The integral form of the energy equation for a control volume (CV) with a diameter *D* and a length *dz* is given by

$$\frac{\boldsymbol{\partial}}{\boldsymbol{\partial t}}\int_{\boldsymbol{CV}}\boldsymbol{E}\,\mathrm{dz}+\int_{\boldsymbol{CV}}\frac{\boldsymbol{\partial \Pi}}{\boldsymbol{\partial z}}\,\mathrm{dz}=\int_{\boldsymbol{CV}}\dot{\boldsymbol{Q}}\,\mathrm{dz}-\int_{\boldsymbol{CV}}\dot{\boldsymbol{W}}\,\mathrm{dz} \quad (2)$$

Where, E is the energy density (energy per unit length) and Π is the energy flux or power, which passes through the ends of the control volume in the axial direction. This energy flux is also known as the instantaneous vibration intensity; $\dot{Q}$ is the rate of work done by the fluid excitation force and $\dot{W}$ is the rate of work done by structural and hydrodynamic sources of damping. Both $\dot{Q}$ and $\dot{W}$ have units of power per unit length.

Basically, the energy equation states that:

$$\begin{bmatrix}\text{time rate of change of}\\ \text{total energy within}\\ \text{the control volume}\end{bmatrix}+\begin{bmatrix}\text{net wave propagation}\\ \text{power flow through}\\ \text{ends of control volume}\end{bmatrix}=$$

$$\begin{bmatrix}\text{net rate of work done by}\\ \text{lift forces on}\\ \text{the control volume}\end{bmatrix}-\begin{bmatrix}\text{net rate of work done}\\ \text{by damping forces}\\ \text{on the control volume}\end{bmatrix} \quad (3)$$

Because all terms in equation (2) are integrals over the same control volume, then equation (2) may be restated in terms of the arguments of the integrals as follows:

$$\frac{\partial E}{\partial t} + \frac{\partial \Pi}{\partial z} = \dot{Q} - \dot{W} \tag{4}$$

Where $\dot{Q}$ is the flow of power into the control volume due to the excitation force and $\dot{W}$ is the power flow due to damping mechanisms. These quantities are difficult to measure.

The left hand side is more tractable. The left hand side is defined as P, where

$$P = \frac{\partial E}{\partial t} + \frac{\partial \Pi}{\partial z} \tag{5}$$

It is possible to evaluate the energy density E and energy flux Π.

Energy density E stored in the riser exists in two basic forms: kinetic energy E_K and potential energy E_P giving

$$E = E_K + E_P \tag{6}$$

Kinetic energy E_K and potential energy E_P can be written as:

$$E_K = \frac{1}{2} m \left(\frac{dv(z,t)}{dt}\right)^2, \quad E_P = \frac{1}{2} T \left(\frac{dv(z,t)}{dz}\right)^2 + \frac{1}{2} EI \left(\frac{d^2 v(z,t)}{dz^2}\right)^2 \tag{7}$$

The energy flux, Π, is the vibration power passing axially along the pipe at the coordinate, z. Energy flux is a measure of the propagation of mechanical power.

$$\Pi(z,t) = -EI \frac{\partial^2 v}{\partial z^2} \frac{\partial \dot{v}}{\partial z} + EI \frac{\partial^3 v}{\partial z^3} \dot{v} - T \frac{\partial v}{\partial z} \dot{v} \tag{8}$$

The energy flux associated with bending waves in a beam is given at any point as the sum of two terms, which will be referred to as the force team and the moment term. The force term is given by the product of the shear force and transverse velocity, shown here as $EI \frac{\partial^3 v}{\partial z^3} \dot{v} — T \frac{\partial v}{\partial z} \dot{v}$. The moment term is given by the product of the bending moment and rotational velocity, shown here as $EI \frac{\partial^2 v}{\partial z^2} \frac{\partial \dot{v}}{\partial z}$. The detailed derivation for energy flux Π can be seen in Appendix 1.

The purpose of this section of the paper is to present a method for identifying the power-in regions of the flexible cylinder excited by the vortex shedding. The quantity p provides the means to do that.

The power-in region is defined as that region where the power generated by the excitation force is greater than the power dissipated by damping. In other words, equation (4) should be greater than zero. To gain a better understanding of the power-in region, it is useful to investigate the time-average of equation (5).

$$\langle P(z,t) \rangle_t = \langle \frac{\partial E}{\partial t} + \frac{\partial \Pi}{\partial z} \rangle_t \tag{9}$$

This is accomplished numerically as follows:

$$\langle P(z,t) \rangle_t = \langle \frac{\partial E}{\partial t} + \frac{\partial \Pi}{\partial z} \rangle_t = \frac{1}{N} \int_0^N \left(\frac{\partial E}{\partial t} + \frac{\partial \Pi}{\partial z} \right) dt \tag{10}$$

Where N is the time duration of the integration.

Energy Density and Flux Estimation

All pipes conducted in the SHELL tests and the EM URC tests were densely instrumented with either strain sensors or both strain sensors and accelerometers at equidistant locations. The measurements, in terms of either strain or acceleration, are not sufficient to estimate energy density and energy flux, as given in equations (6) and (8). For a beam, one must obtain accurate estimates of the first, second, third and fourth spatial derivatives of the flexural displacement, $v(z,t)$ in order to estimate the energy density and energy flux.

In this paper, the time histories of flexural displacement $v(z,t)$ could be obtained through modal analysis, in which curvature mode shapes are used to identify modal weights. Once the modal weight of displacement is obtained, the corresponding slope $\frac{\partial v(z,t)}{\partial z}$, curvature $\frac{\partial^2 v(z,t)}{\partial z^2}$, third spatial derivative $\frac{\partial^3 v(z,t)}{\partial z^3}$, and fourth spatial derivative $\frac{\partial^4 v(z,t)}{\partial z^4}$ at all points of the pipe could be obtained from the known relationships between displacement mode shapes and the mode shapes for slope, curvature, third and fourth spatial derivatives (Rao at el.,2012).

RESULTS

• Using Test 2331 to Benchmark the Power-In Region Identification Methodology

Figure 5. Schematic of Pipe 1 with fairings at two ends of the pipe, leaving a gap (bare region) in the centre

Figure 5 shows the schematic of Pipe 1 with the two ends partially covered by fairings and a bare region in the centre of the pipe. For this pipe with partial coverage of ribbon fairings in uniform flow, the bare section is very likely to be power-in region and the section with fairing is very likely to be a power-out region. Figure 3 clearly indicates that waves emanate from the bare region and travel into the faired regions. Thus, this pipe is a good case to benchmark the power-in region identification methodology.

Test 2331 was chosen to demonstrate how this methodology works in identifying the power-in region. For this test, the bare region in the centre is 15% of the pipe. It is expected that the identified power-in region is from z/L= 0.425 to 0.575.

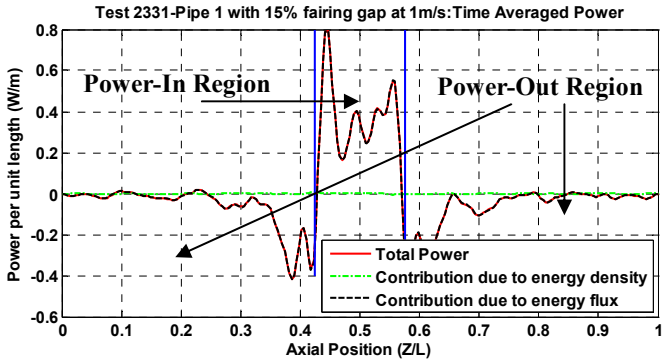

Figure 6. The time-average power for Test 2331 with 15% fairing gap in the center of the pipe at 1m/s from 71-74 seconds.

Figure 6 shows the estimated power per unit length along the pipe for test 2331. The red line is the estimated time average total power $\langle P(z,t)\rangle_t$ from equation (10) and the black dashed line is the contribution due to the energy flux $\langle\frac{\partial \Pi}{\partial z}\rangle_t$ and the green solid line is the contribution due to the energy density $\langle\frac{\partial E}{\partial t}\rangle_t$. Fig.6 also shows that the power due to the contribution of the energy flux is dominant and the power due to the contribution of the energy density is almost zero. This is because at steady state, the average energy stored in the control volume is constant.

Two vertical blue lines are the boundaries of bare region in the centre of the pipe which is from 0.425 to 0.575. The total time average power indicates the location of power-in region. The regions with positive and negative time-average total power are the power-in region and power-out region respectively. Positive power means that the power generated by the flow is greater than that dissipated by the damping in the same region. This is illustrated very clearly in Fig.6 in which the identified power-in region is from 0.4257 to 0.5743 which matches well with the region lacking fairings.

Figure 6 suggests that the power due to the contribution of the energy flux is overwhelmingly dominant and the identified power-in region matches well with the region lacking fairings. But from the information in equation (5) there is no way to tell the direction of wave propagation from the total time-average power.

Figure 7 shows the time average energy flux $\langle \Pi\rangle_t$ in red line for test 2331. And the two vertical blue lines are the boundaries of bare region in the centre of the pipe. The advantage of this plot is that it indicates the direction of wave propagation. Negative time-average energy flux suggests the energy transfers from right to left and waves propagate from right to left as indicated by the blue arrow. While positive time-average energy flux suggests waves carrying energy from the power-in region propagate from left to right as indicated by the black arrow. The observation agrees well with the contour plot in Fig.4. It is noted that the dominant mode number is 23 and 3 half-wavelengths are equal to the length of the power-in region.

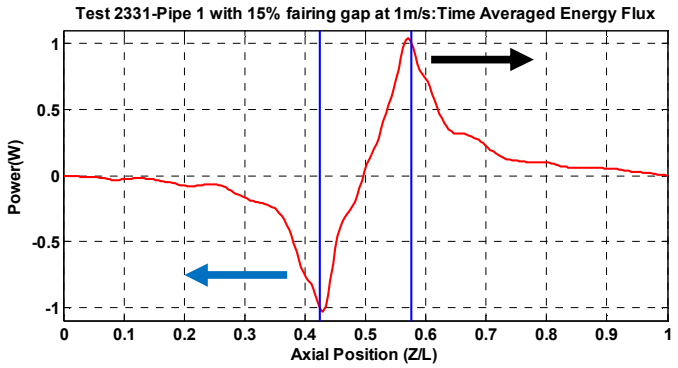

Figure 7. The time-average energy flux for Test 2331 with 15% fairing gap in the center of the pipe at 1m/s from 71-74 seconds.

• Power-In Region Identification for Pipe 1 with Partially Covered Fairings under Uniform Flows

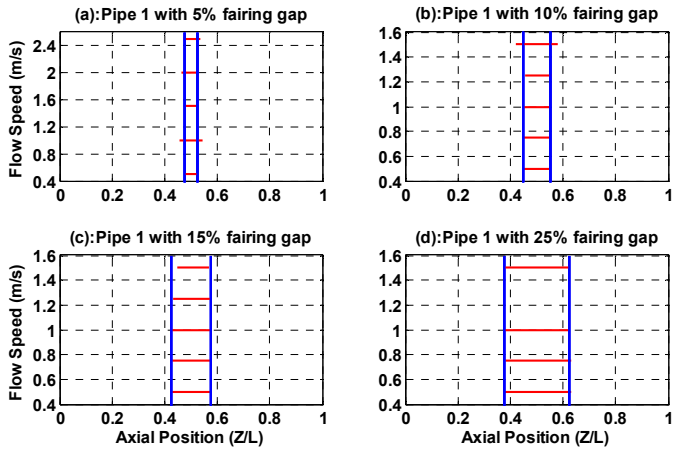

Figure 8. Experimentally determined power-in regions for Pipe 1 in uniform flows, centrally located gap lengths of 5%, 10%, 15% and 25%.

Figure 8 shows the power-in regions identified by this method for four different exposed lengths at many different flow speeds. For example, the data in Fig.6 is shown as a red bar at 1m/s for the 15% gap length in Fig.8.

In each figure the two vertical blue lines are the boundaries of the fairing gap for each case. Fig.8 (a)-(d) represents Pipe 1 with 5%, 10%, 15% and 25% fairing gap respectively. The horizontal red bars are the experimentally determined power-in regions at each flow speed. Figs.8 show that the identified power-in regions match well with the fairing gaps on Pipe 1.

The dominant mode number is changing from test to test because of the different flow speed and tension for each test. The number of half wavelengths in the fairing gap is from 1 to 3. Now we have demonstrated a method for identifying power-in regions. It is next applied to several more difficult cases.

• Power-In Region Identification for Completely Bare Pipes under Sheared Flow

For the completely bare pipe under sheared flow, it is expected that the power-in region will be at the higher flow speed end. But what portion of the pipe is the power-in region?

For Bare Pipe 1 with linearly sheared flow the higher flow speed end is at *Z/L=0.* Figure 9 shows the identified power-in regions at different flow speeds, using equation (10). Here the "flow speed" in Fig.9 is the maximum flow velocity. The horizontal red bars represent the identified power-in regions. As expected, the power-in regions are at higher flow speed ends. The average length of all these power-in regions is 34.5% of the whole pipe.

The dominant modes for all tests ranged from 8 to 28 and the number of half wavelengths in the identified power-in region ranged from 3 to 10. It is also found that the start and end points of the power-in regions varied slightly from test to test. Specifically, the power-in regions for the high speed tests do not extend all the way to the boundary. This is attributed to the fact that the reduced velocity at the high speed end (*Z/L*=0) was outside the reduced velocity lock-in band for the dominant excited mode.

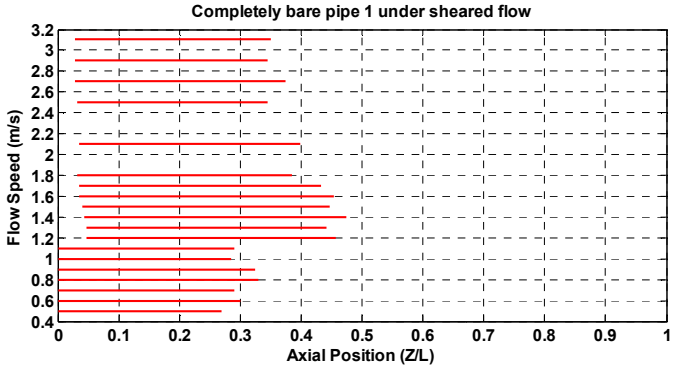

Figure 9. Identified power-in regions for completely bare Pipe 1 under sheared flow. *Z/L*=0 is at the higher flow speed end.

The methodology was also applied to the identification of the power-in region for Pipe 3 covered with both strakes and marine growth. The results are shown in appendices 2.1, 2.2, and 2.3.

INVESTIGATION IN THE SECONDARY POWER-IN REGION

Figure 10 shows the schematic of Pipe 4 with four strake configurations in linearly sheared flow. Pipe 4 had a diameter of 20 mm and a length of 9.63m. Fig.10 (a) is the completely bare Pipe 4 and the expected power-in region "*Lin*" is at the higher flow speed end which is labeled with red color. Subsequently, 25% strakes are put at the higher flow speed end to suppress the primary power-in region found in Fig.10 (a) and to explore the occurrence of the secondary power-in region. Then additional 25% strakes are added to Fig.10 (b) to reach a total of 50% strakes coverage in order to study whether the secondary power-in region will be suppressed and the tertiary power-in region will be found. At the end, a total of 75% strakes are installed to study the occurrence of the quaternary power-in region.

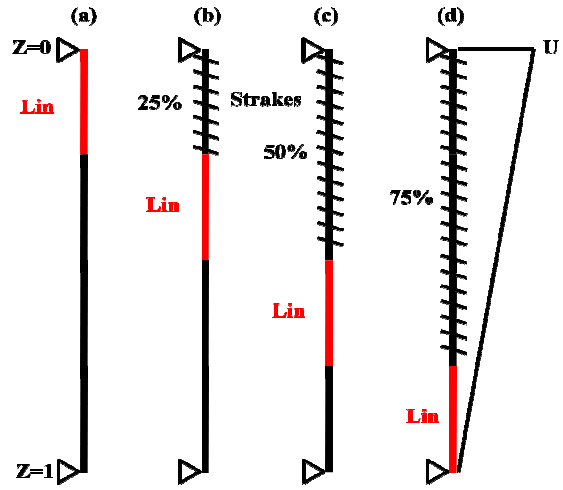

Figure 10. Schematic of Pipe 4 with four strake configurations under linearly sheared flow. The higher flow speed end is at *Z/L* coordinates of 0. (a) completely bare Pipe 4; (b) Pipe 4 with 25% strakes at higher flow speed; (c) Pipe 4 with 50% strakes at higher flow speed; (d) Pipe 4 with 75% strakes at higher flow speed

• Power-In Region Identification for Completely Bare Pipe 4 under Sheared Flow

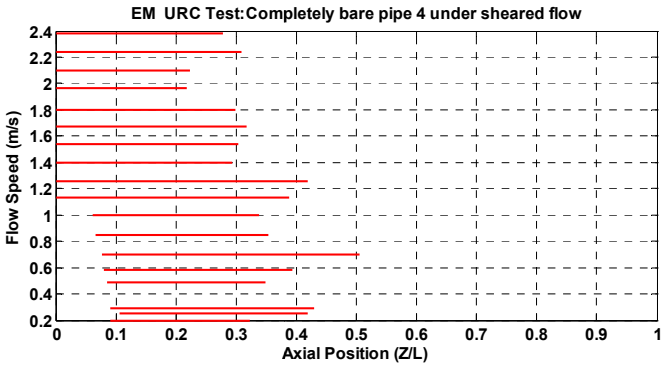

Figure 11. Identified power-in region for completely bare Pipe 4 under sheared flow from EM URC test

The higher flow speed end is also at *Z/L* coordinates of 0. As was found for Pipe 1 in sheared flow and shown in Fig.9, the power-in region is found to be located at higher flow speed end. The horizontal red bars were the identified power-in regions at different flow speeds. The bound of the power-in region varied from test to test. The average length of all these power-in regions is 30.6% of the whole pipe which is somewhat shorter than that shown in Fig.9 for Pipe 1.

The dominant modes for all tests ranged from 1 to 7 and the number of half wavelengths in the identified power-in region ranged from 0.2 to 2. The power-in regions for the low speed tests do not extend all the way to the boundary. It may attribute to the fact that a large error is introduced into response reconstruction for the cases dominated by first mode response (Lie and Kaasen, 2006), these were all cases with flow speed below 1.2m/s. Waves with a wavelength longer than the power-in region still propagate but the response may be dominated by a standing wave.

• Power-In Region Identification for Pipe 4 with 25% Strakes in Higher Flow Speed End

For completely bare Pipe 4 under sheared flow, the power-in region is found to be at the higher flow speed end. It is interesting to investigate whether a secondary power-in region occurs if suppression is placed in the primary power-in region. In EM URC test, 25% strake coverage was put in the higher flow speed end. It was expected that the region with 25% strakes would be a power-out region and the primary power-in region would be suppressed.

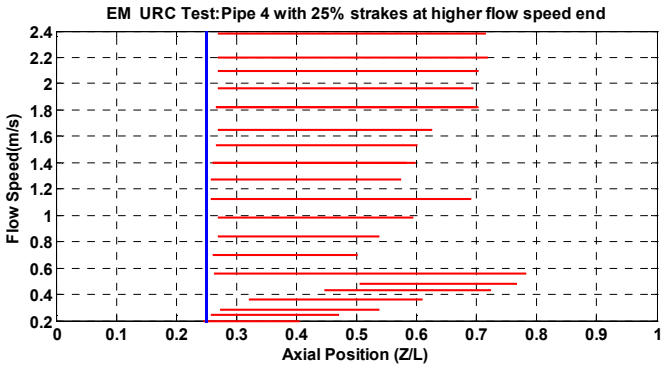

Figure 12. Identified power-in region for Pipe 4 with 25% strakes at higher flow speed under sheared flow

Figure 12 shows the experimentally determined power-in regions using the proposed methodology for Pipe 4 with 25% strakes under linearly sheared flow. The vertical blue line is at *Z/L* coordinates of 0.25 which is the right boundary of the strakes. Fig.12 clearly indicates that the original primary power-in region becomes the power-out region. A secondary power-in region appears which is represented by the horizontal red lines. Secondary power-in region also changes from test to test. The average length of these secondary power-in regions at all these flow speeds is 34.3% of the whole pipe.

• Power-In Region Identification for Pipe 4 with 50% Strakes in Higher Flow Speed End

After suppressing the primary power-in region with 25% strakes at the higher flow speed end, the secondary power-in region is observed in Fig.12. After an additional 25% strakes were added into the higher flow speed end, the strake coverage is 50%. A vertical blue line is the right boundary of the 50% strakes. It was expected that the left region with 50% strakes would become the power-out region.

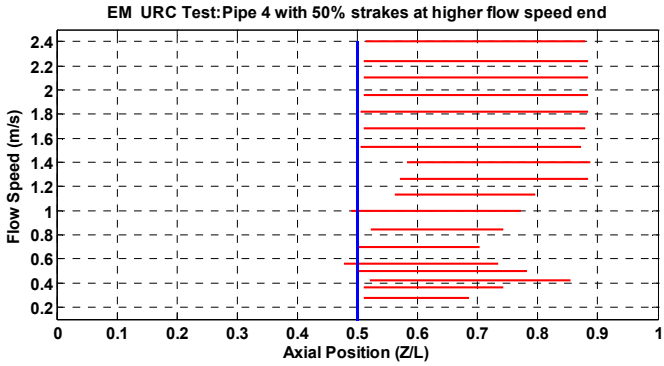

Figure 13. Identified power-in region for Pipe 4 with 50% strakes at the higher flow speed under sheared flow

Figure 13 shows the identified power-in regions in horizontal red lines at different flow speeds. From Fig.13, no power-in region is found in the straked region. It indicates that the secondary power-in region in Fig.12 is fully suppressed by strakes. The tertiary power-in region appears. The tertiary power-in region changed from test to test. The average length of these tertiary power-in regions at all these flow speeds is 28.7% of the whole pipe.

• Power-In Region Identification for Pipe 4 with 75% Strakes at the Higher Flow Speed End

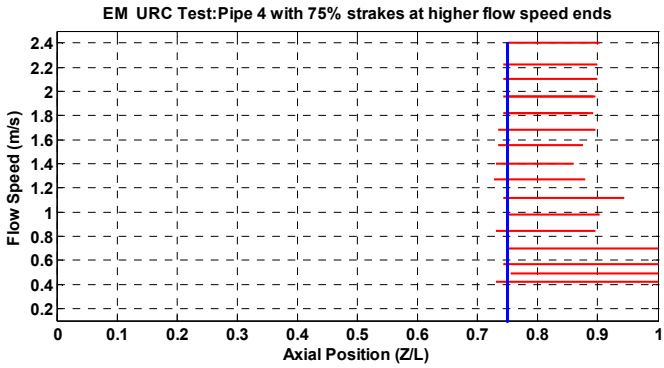

Figure 14. The identified power-in region for Pipe 4 with 75% strakes at the higher flow speed under sheared flow

The tertiary power-in region was observed after suppressing both primary and secondary power-in regions. An additional 25% strakes were added into the higher flow speed end to see whether a quaternary power-in region would exist. At this point the total strake coverage is 75% and a vertical blue line in Fig.14 represents the right boundary of the 75% strakes.

Fig.14 shows the identified power-in regions for Pipe 4 with 75% strakes in the left hand side under linearly sheared flow. The horizontal red bars represent the identified power-in region at different flow speeds. Still, no power-in region is found in the straked region. All these figures show that this kind of strake is effective in suppressing VIV. The power-in region observed in Fig.14 started from the right boundary of the straked region. The power-in region is almost the entire bare region except the higher flow speed cases. The average length of these quaternary power-in regions at all these flow speeds is 19.5% of the whole pipe.

From Figs.12 to 14, the region at the higher flow speed end is favored to be the power-in region. When the higher flow speed region is suppressed with strakes, the next higher flow speed region becomes the power-in region. When strakes are installed continuously in the higher flow speed region, the end of straked region is usually the starting point of the power-in region. The pipe may be excited at low flow speed even though the bare region is small. In other words, VIV will be observed if the pipe is not fully straked.

• Effect of Power-In Region Location on VIV Amplitude

The power-in regions were identified for all four pipes mentioned above at all flow speeds. The average power-in length for these four pipes is around 30% of the whole pipe. But these power-in regions are at different locations for different flow speeds. What's the effect of these power-in regions which are of the same length but act at different locations?

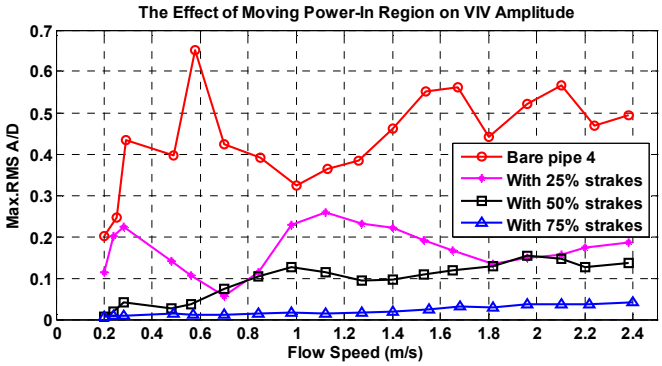

Figure 15. Effect of power-in region locations on VIV amplitude

Figure 15 shows maximum RMS displacement along the riser versus maximum flow speeds for four pipes. They are completely bare Pipe 4, Pipe 4 with 25% strakes, Pipe 4 with 50% strakes and Pipe 4 with 75% strakes. The red line with red circles represents the maximum RMS *A/D* for the completely bare pipe 4. The maximum *A/D* fluctuated with flow speed in the range of 0.2 to 0.7. The average maximum RMS *A/D* at all flow speeds is around 0.437. When 25% strakes are installed at higher flow speed end, the VIV amplitude in magenta lines with magenta stars reduces abruptly. That's because strakes behave like a damper which dissipates the energy from the power-in region. Meanwhile the placement of strakes also forces the power-in region move to low flow speed region. The average maximum RMS *A/D* at all flow speeds becomes 0.170. The 25% strakes caused near 60% VIV amplitude drop. When additional 25% strakes are added to the pipe, the VIV amplitude black lines with black squares doesn't decrease too much, its average maximum RMS *A/D* at all flow speeds is around 0.092 which means 50% strakes cause an 80% VIV amplitude drop. When another additional 25% strakes are put in the pipe, the VIV amplitude in blue lines with blue triangles is negligible. The average maximum *A/D* at all flow speeds decreases to 0.021.

• Effect of Power-In Region Location on Damage Rate

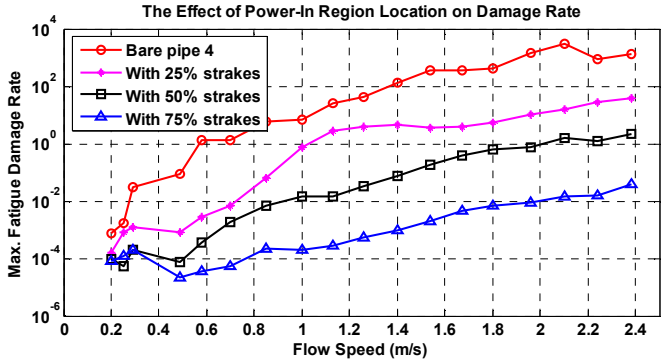

Figure 16. Effect of power-in region locations on fatigue damage rate

Moving the power-in region by means of partial strake coverage has an effect on fatigue damage rate. This effect was investigated with the rainflow counting method. The analysis uses the Wave Analysis for Fatigue and Oceanography (WAFO) (WAFO, 2006) MATLAB toolbox developed by Lund Institute of Technology in Sweden to perform rainflow cycle counting and to estimate fatigue damage rate. For these predictions the pipe was assumed to be steel and with material properties given by the DNV F-2 S-N curve (b=3.0 and C=4.268x10^{11} (MPa)^3).

Figure 16 shows maximum fatigue damage rate along the riser versus maximum flow speeds for four pipes. Power-in regions for these four pipes have similar length but are at different locations on the pipe. From Fig.18, as expected, bare Pipe 4 has the highest fatigue damage rate compared to pipes with other strake coverage. Pipe 4 with 25% and 50% strakes have the second and third-highest fatigue damage rate respectively and Pipe 4 with 75% strake has lowest fatigue damage rate.

Compared to the bare Pipe 4, Pipe 4 with 25%, 50% and 75% strakes have 1-2, 2-3 and 5-6 orders of magnitude lower fatigue damage rate respectively. The fatigue damage rate reduction is in part due to the fact that there is less energy in partially straked Pipe 4 with a given maximum velocity than bare Pipe 4. The lower energy in straked Pipe 4 is due to the power-in region being at lower flow speed which results in smaller VIV amplitude with lower excitation frequency and lower responding mode number.

The identification of the power-in region for pipes under sheared flow is useful for riser design. It can provide guidance on both strake installation and repair. For example, for a completely bare pipe under sheared flow, one may estimate the amount of strake coverage needed to decrease the average response *A/D* by half or reduce the fatigue damage rate by one order of magnitude. Or for a completely straked pipe, these results provide guidance on what portion of strakes can be damaged or fouled before the average *A/D* increases to a point requiring repair.

CONCLUSIONS

The primary contribution of this work was to identify the power-in region based on energy conservation and to study the occurrence of secondary power-in regions if suppression devices are placed in the primary power-in zone. Preliminary conclusions from the power-in region identification include:

(1) Based on energy conservation, the paper developed a method to find power-in regions for flexible risers.

(2) For pipes partially covered with suppression devices, like fairings, the identified power-in regions match well with fairing gaps.

(3) For bare pipes under sheared flow, it was found that the power-in region is always at the higher flow speed end. The length of the power-in region is around 30% of the entire pipe.

(4) The paper also explored the occurrence of secondary power-in regions after suppression is placed in the primary power-in zone. The secondary power-in region was observed and no power-in regions were found in the straked region in EM URC test. This study will be useful in providing guidance for strake installation or repairs.

ACKNOWLEDGMENTS

The authors gratefully acknowledge Deepstar and the SHEAR7 JIP members (BP, Chevron, ConocoPhillips, ExxonMobil, Petrobras, Shell, Statoil & Technip) for supporting this research, and especially SHELL Exploration and Production for providing access to the data and ExxonMobil Upstream Research Center for providing the use of their data.

REFERENCES

Campbell, B. and Slocum, S.T., 2013. Prediction of VIV for risers with effective strakes. In: Proceedings of the 32nd OMAE. Nantes, France, Paper no.11413.

Jhingran, V., Zhang, H., Lie, H., Bratton, H. and Vandiver, J.K., 2012. Buoyancy spacing implications for fatigue damage due to vortex-induced vibrations on a steel lazy wave riser (SLWR). In: Proceedings of the OTC. Paper no. 23672.

Lie, H. and Kaasen, K.E., 2006. Modal analysis of measurements from a large-scale VIV model test of a riser in linearly sheared flow. Journal of Fluids and Structures, Vol. 22, pp.557-575.

MARINTEK, 2011. Shell Riser VIV Tests Main Report. Main report No.580233.00.01. Norwegian Marine Technology Research Institute.

Noiseux, D.U., 1970. Measurement of power flow in uniform beams and plates. Journal of the Acoustical Society of America, Vol. 47, No. 1, pp.238-247.

Pavic, G., 1976. Measurement of structure borne wave intensity. Journal of Sound and Vibration, Vol. 49, No. 2, pp. 221-230.

Rao, Z., Vandiver, J.K. & Jhingran, V., 2013. VIV excitation competition between bare and buoyant segments of flexible cylinders. In: Proceedings of the 32nd OMAE. Nantes, France, Paper no. 11296.

Rao, Z., Vandiver, J.K., Jhingran, V. & Sequeiros, O., 2012. The effect of exposure length on vortex induced vibration of flexible cylinders. In: Proceedings of the 31st OMAE. Rio de Janeiro, Paper no. 83273.

Resvanis, T.L., Jhingran, V. & Vandiver, J.K., 2012. Reynolds number effects on the vortex-induced vibration of flexible marine risers. In: Proceedings of the 31st OMAE. Rio de Janeiro, Paper no. 83565.

Resvanis, T.L., Rao, Z. & Vandiver, J.K., 2014. Effects of strake coverage and marine growth on flexible cylinder VIV. In: Proceedings of the 33rd OMAE, San Francisco, CA, USA, Paper no.24462.

Swithenbank, S.B. and Vandiver, J.K., 2007. Identifying the power-in region for vortex-induced vibrations of long flexible cylinders. In: Proceedings of the 26th OMAE, San Diego, California, USA, Paper no. 29156.

Tognarelli, M.A., Slocum, S.T., Frank, W.R. and Campbell, R.B., 2004. VIV response of a long flexible cylinder in uniform and linearly sheared currents. In: Proceedings of the OTC. Paper no. 16338.

WAFO, 2006. Wave Analysis for Fatigue and Oceanography. Homepage, Lund Institute of Technology, http://www.maths.lth.se/matstat/wafo/.

APPENDIX 1

Instantaneous Vibration Intensity (Energy Flux)

The instantaneous vibration intensity is the vibration power passing through a cross-sectional area of a structure. It is defined as the stress traction vector on the surface of the cylinder cross-section times the velocity of the same cross-section. Vibration intensity is a measure of mechanical power transmission and propagation. Vibration intensity was first introduced by Noiseux (1970) and later developed by Pavic (1976).

Consider an Euler – Bernoulli beam of a cross-section $A(z)$ under tension T, undergoing in-line vibration $u(z,t)$ and cross-flow vibration $v(z,t)$ with E being Young's modulus, the displacement vectors u, v, w in x, y, z axes are defined by:

$$u = u(z,t) \tag{A.1}$$

$$v = v(z,t) \tag{A.2}$$

$$w = -x\frac{\partial u}{\partial z} - y\frac{\partial v}{\partial z} + \frac{Tz}{EA} \tag{A.3}$$

Where x, y, z are the coordinate axes axially in the in-line direction, in the cross-flow direction and along the pipe respectively. Stresses are expressed in the following formulas:

$$\sigma_{zx} = \frac{(R^2 - x^2)\left(-EI\frac{\partial^3 u}{\partial z^3} + T\frac{\partial u}{\partial z}\right)}{3I} \tag{A.4}$$

$$\sigma_{zy} = \frac{(R^2 - y^2)\left(-EI\frac{\partial^3 v}{\partial z^3} + T\frac{\partial v}{\partial z}\right)}{3I} \tag{A.5}$$

$$\sigma_{zz} = -Ey\frac{\partial^2 v}{\partial z^2} - Ex\frac{\partial^2 u}{\partial z^2} + \frac{T}{A} \tag{A.6}$$

Where R, I are the radius of the pipe and the second moment of area, respectively. The instantaneous vibration intensity in the axial, z, direction is expressed by:

$$\Pi_z(x,y,z,t) = -\sigma_{zx}\dot{u} - \sigma_{zy}\dot{v} - \sigma_{zz}\dot{w} \tag{A.7}$$

The total vibration intensity at a cross-section is thus given by:

$$\Pi_z(z,t) = \iint \Pi_x(x,y,z,t)dxdy \tag{A.8}$$

Substitute equations (A.4), (A.5), (A.6) and (A.7) into the equation (A.8), yields

$$\iint -\sigma_{zx}\dot{u}dxdy = EI\frac{\partial^3 u}{\partial z^3}\dot{u} - T\frac{\partial u}{\partial z}\dot{u} \tag{A.9}$$

$$\iint -\sigma_{zy}\dot{v}dxdy = EI\frac{\partial^3 v}{\partial z^3}\dot{v} - T\frac{\partial v}{\partial z}\dot{v} \tag{A.10}$$

$$\iint -\sigma_{zz}\dot{w}dxdy = -EI\frac{\partial^2 u}{\partial z^2}\frac{\partial \dot{u}}{\partial z} - EI\frac{\partial^2 v}{\partial z^2}\frac{\partial \dot{v}}{\partial z} \tag{A.11}$$

Thus, the total vibration intensity at a cross-section becomes

$$\Pi_z(z,t) = -EI\frac{\partial^2 u}{\partial z^2}\frac{\partial \dot{u}}{\partial z} + EI\frac{\partial^3 u}{\partial z^3}\dot{u} - T\frac{\partial u}{\partial z}\dot{u} - EI\frac{\partial^2 v}{\partial z^2}\frac{\partial \dot{v}}{\partial z} + EI\frac{\partial^3 v}{\partial z^3}\dot{v} - T\frac{\partial v}{\partial z}\dot{v} \tag{A.12}$$

The instantaneous vibration intensity in equation (A.12) is for bending waves in both cross-flow and in-line directions. In the cross-flow direction, the instantaneous vibration intensity associated with bending waves in a beam is given at any point as the sum of two terms, which will be referred to as the force team and the moment term. The force term is given by the product of the shear force and transverse velocity, shown here as $EI\frac{\partial^3 v}{\partial z^3}\dot{v}$— $T\frac{\partial v}{\partial z}\dot{v}$. The moment term is given by the product of the bending moment and rotational velocity, shown here as $EI\frac{\partial^2 v}{\partial z^2}\frac{\partial \dot{v}}{\partial z}$.

In this paper, vibration only in the cross-flow direction is considered. Thus, the total vibration intensity at any point in cross-flow direction becomes:

$$\Pi_{z-CF}(z,t) = -EI\frac{\partial^2 v}{\partial z^2}\frac{\partial \dot{v}}{\partial z} + EI\frac{\partial^3 v}{\partial z^3}\dot{v} - T\frac{\partial v}{\partial z}\dot{v} \tag{A.13}$$

APPENDIX 2

• Appendix 2.1: Pipe 3 Fully Covered with both Strakes and 30% Marine Growth under Sheared Flow

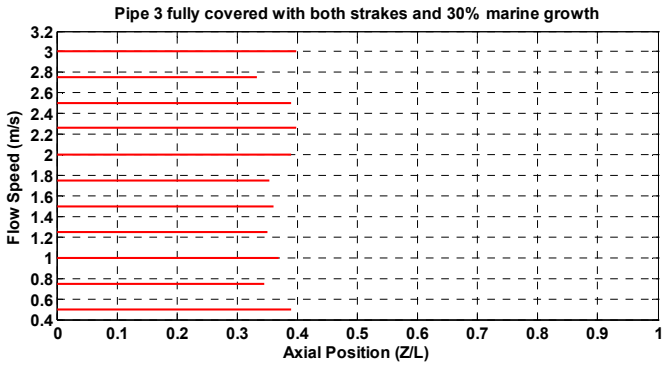

Appendix 2.1. Identified power-in region for Pipe 3, fully covered with strakes with marine growth under sheared flow. Marine growth is 30% of strake height

Appendix 2.1 and 2.2 show the identified power-in regions for fully straked Pipe 3 with 30% and 60% marine growth respectively. The power-in regions are clearly observed at the higher flow speed end. This kind of helical strake is well known to be effective in suppressing VIV. However, when the straked

regions are covered with either 30% or 60% marine growth, the effectiveness of the strakes is highly reduced.

• Appendix 2.2: Pipe 3 Fully Covered with both Strakes and 60% Marine Growth under Sheared Flow

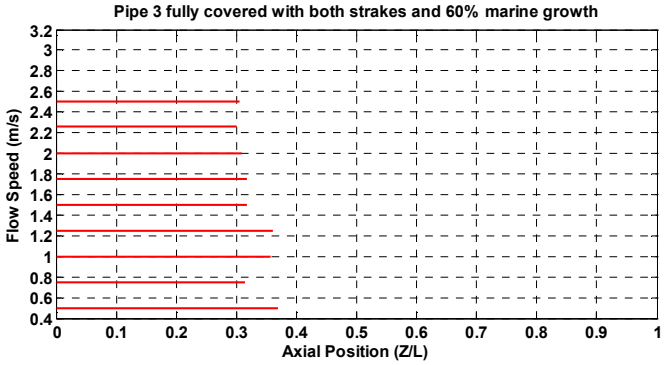

Appendix 2.2. Identified power-in region for Pipe 3, fully covered with strakes with marine growth under sheared flow. Marine growth is 60% of strake height

• Appendix 2.3: Fully Straked Pipe 3, 60% of Strakes Covered with 60% High Marine Growth in Sheared Flow

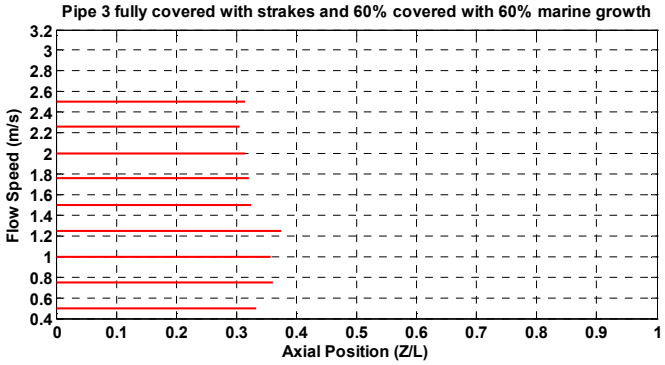

Appendix 2.3. Identified power-in region for Pipe 3, fully covered with strakes with marine growth under sheared flow. 60% high marine growth on the left 60% of the pipe in sheared flow

Appendix 2.3 shows the identified power-in regions for fully straked Pipe 3 but partially covered with marine growth. The left 60% of the straked Pipe 3 was covered by marine growth and left the right 40% with only strakes. The identified power-in regions here are almost the same as those in Pipe 3 fully covered with both strakes and marine growth. That's because the power-in regions are at higher flow speed end for such pipe under sheared flow and the length of the power-in region is usually less than 60%.